Winter 1-18-2016

Synthesis, Characterization, and Thin-Film Properties of 6-Oxoverdazyl Polymers Prepared by Ring-Opening Metathesis Polymerization

Joseph A. Paquette

Sabastine Ezugwu

Vishal Yadav

Giovanni Fanchini

Joe Gilroy
jgilroy5@uwo.ca

Synthesis, Characterization, and Thin-Film Properties of 6-Oxoverdazyl Polymers Prepared by Ring-Opening Metathesis Polymerization

Joseph A. Paquette,[1,2] Sabastine Ezugwu,[2,3] Vishal Yadav,[2,3] Giovanni Fanchini,*[1,2,3] and Joe B. Gilroy*[1,2]

[1]Department of Chemistry and [2]The Centre for Advanced Materials and Biomaterials Research (CAMBR), The University of Western Ontario, London, ON, Canada, N6A 5B7. [3]Department of Physics and Astronomy, The University of Western Ontario, London, ON, Canada, N6A 3K7. E-mail: gfanchin@uwo.ca, joe.gilroy@uwo.ca

ABSTRACT: Redox-active 6-oxoverdazyl polymers were synthesized via ring-opening metathesis polymerization (ROMP) and their solution, bulk, and thin-film properties investigated. Detailed studies of the ROMP method employed confirmed that stable radical polymers with controlled molecular weights and narrow molecular weight distributions ($Đ$ < 1.2) were produced. Thermal gravimetric analysis of a representative example of the title polymers demonstrated stability up to 190 °C, while differential scanning calorimetry studies revealed a glass transition temperature of 152 °C. Comparison of the spectra of 6-oxoverdazyl monomer **12** and polymer **13**, including FT-IR, UV-vis absorption, and electron paramagnetic resonance spectroscopy, was used to confirm the tolerance of the ROMP mechanism for the 6-oxoverdazyl radical both qualitatively and quantitatively. Cyclic voltammetry studies demonstrated the ambipolar redox properties of polymer **13** ($E_{1/2,ox}$ = 0.25 and $E_{1/2,red}$ = −1.35 V relative to ferrocene/ferrocenium), which were consistent with those of monomer **12**. The charge transport properties of thin films of polymer **13** were studied before and after a potential of 5 V was applied, revealing a drastic drop in the resistivity from 10^6–10^{10} Ω·m or more to 1.7×10^4 Ω·m and suggesting the potential usefulness of polymer **13** in bistable electronics.

KEYWORDS: stable radical polymers; ring-opening metathesis polymerization; polymer thin-films; semiconductivity, EPR spectroscopy.

INTRODUCTION

Functional polymers with potentially useful optical and electronic properties have received significant attention due to the ability of these materials to improve upon existing technologies by combining the unique properties of small functional molecules (*e.g.*, electron transfer, light absorption/emission, magnetic) with the processability, mechanical robustness, and flexibility associated with polymers.[1] An interesting subclass of functional polymers that has emerged in recent years contain stable organic radicals[2] in the repeating unit pendant to their backbones.[3-5] The vast majority of research towards stable radical polymers has been motivated by their utility as electrode materials in batteries,[3-4,6] where the introduction of conductive (nano)fillers has led to enhanced performance.[7-10] However, radical polymers have also shown application as high-spin ground state materials,[11] (co)catalysts for the selective oxidation of alcohols,[12] inhibitors of self-polymerization reactions,[13] solid-state conductive materials,[14-16] and the functional component of memory architectures.[17-19]

The most widely studied family of stable radical polymers is based on 2,2,6,6-tetramethyl-piperidin-1-yl (TEMPO, **1**) radicals,[15,20-28] while examples based on other families of radicals, including nitronyl nitroxide (**2**),[29] 2,2,5,5-tetramethyl-1-pyrrolidinylloxy (PROXYL, **3**),[30] spirobisnitroxide (**4**),[31] aminoxy (**5**),[32] galvinoxyl (**6**),[33] and 6-oxoverdazyl (**7**)[34] radicals have received considerably less attention (Figure 1). Further expansion of the stable radical polymer field to include examples based on these and other stable radicals will allow for the realization of materials with targeted properties that are suitable for the applications described above. 6-Oxoverdazyl radicals offer exceptional stability towards air and moisture, and, while their high molecular weights render them poor candidates for battery applications, their tunable ambipolar redox properties[34-35] may allow for their future use as charge transport materials.

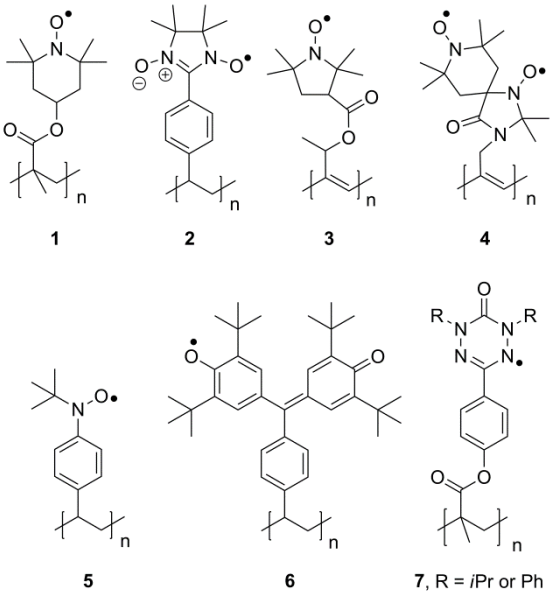

FIGURE 1 Representative examples of stable radical polymers.

Most synthetic protocols, for example those targeting nitroxide radical polymers, involve the polymerization of monomers based on radical precursors followed by post-polymerization reactions designed to generate the targeted stable radical polymers. These strategies are often hampered by difficulty surrounding the complete conversion of the radical precursor repeating units to their stable radical form, a factor that has recently been shown to affect their charge transport properties.[16] Therefore, there remains a need for further development of polymerization protocols that allow for direct polymerization[26,36-40] of stable radical-containing monomers and ensure a high degree of radical content along the polymer backbone.

Herein, we report the ring-opening metathesis polymerization (ROMP) behavior of a 6-oxoverdazyl radical monomer and the thorough characterization of the bulk, solution, and thin-film properties of the resulting polymers.

EXPERIMENTAL

General

All reactions and manipulations were carried out under a nitrogen atmosphere using standard Schlenk techniques unless otherwise stated. Solvents were obtained from Caledon Laboratories, dried using an Innovative Technologies Inc. solvent purification system, collected under vacuum, and stored under a nitrogen atmosphere over 4 Å molecular sieves. All reagents were purchased from Sigma-Aldrich, Alfa Aesar, or Oakwood Chemicals and used as received unless otherwise stated. 2,4-Di-*iso*propylcarbonohydrazide bis-hydrochloride **8**[41] and *N*-(3-hydroxylpropyl)-*cis*-5-norbornene-*exo*-2,3-dicarboximide **11**[42] were prepared according to published procedures. NMR spectra were recorded on a 400 MHz (^{1}H: 400.1 MHz, ^{13}C: 100.4 MHz) Varian INOVA instrument. ^{1}H NMR spectra were referenced to residual CD_3SOCD_2H (2.50 ppm) and ^{13}C {^{1}H} NMR spectra were referenced to CD_3SOCD_3 (39.5 ppm). Mass spectrometry data were recorded in positive-ion mode using a high resolution Finnigan MAT 8200 spectrometer using electron impact ionization. UV-vis absorption spectra were recorded in CH_2Cl_2 solutions using a Cary 300 Scan instrument. Four separate concentrations were run for each sample, and molar extinction coefficients were determined from the slope of a plot of absorbance against concentration. FT-IR spectra were recorded on a PerkinElmer Spectrum Two FT-IR as KBr pellets. Elemental analysis (C, H, N) was carried out by Laboratoire d'Analyse Élémentaire, Université de Montréal, Montréal, QC, Canada.

Gel Permeation Chromatography (GPC)

GPC experiments were conducted in chromatography grade THF at concentrations of 5 mg mL^{-1} using a Viscotek GPCmax VE 2001 GPC instrument equipped with an Agilent PolyPore guard column (PL1113-1500) and two sequential Agilent PolyPore GPC columns

packed with porous poly(styrene-*co*-divinylbenzene) particles (MW range 200−2,000,000 g mol^{-1}; PL1113-6500) regulated at a temperature of 30 °C. Signal response was measured using a Viscotek VE 3580 RI detector, and molecular weights were determined by comparison of the maximum RI response with a calibration curve (10 points, 1,500–786,000 g mol^{-1}) established using monodisperse polystyrene purchased from Viscotek.

Thermal Analysis

Thermal degradation studies were performed using a TA Instruments Q600 SDT TGA and processed using TA Universal Analysis software. Samples were placed in an alumina cup and heated at a rate of 10 °C min^{-1} from 25 to 800 °C under a flow of nitrogen (100 mL min^{-1}). Glass transition temperatures were determined using differential scanning calorimetry (DSC) on a TA Instruments DSC Q20. The polymer samples were placed in an aluminum Tzero pan and heated from room temperature to 180 °C at a scan rate of 10 °C min^{-1} under a flow of nitrogen (50 mL min^{-1}) and cooled down to 0 °C at a scan rate 10 °C min^{-1} before they underwent two more heating/cooling cycles. The glass transition temperature (T_g) was determined from the second heating/cooling cycle.

Cyclic Voltammetry (CV)

CV experiments were performed with a Bioanalytical Systems Inc. (BASi) Epsilon potentiostat and analyzed using BASi Epsilon software. Typical electrochemical cells consisted of a three-electrode setup including a glassy carbon working electrode, platinum wire counter electrode, and silver wire *pseudo*-reference electrode. Experiments were run at 100 mV s^{-1} in degassed $MeCN/CH_2Cl_2$ (1:1) solutions of the analyte (~1 mM) and electrolyte (0.1 M nBu_4NPF_6). Voltammograms were referenced internally against the ferrocene/ferrocenium redox

couple (~1 mM internal standard) and corrected for internal cell resistance using the BASi Epsilon software.

Electron Paramagnetic Resonance (EPR) Spectroscopy

EPR measurements were made on *ca.* 10^{-5} M CH_2Cl_2 solutions of 6-oxoverdazyl monomer **12** and polymer **13** that had been subjected to three freeze-pump-thaw cycles in 0.4 mm quartz tubes using a JEOL JES-FA200 EPR spectrometer. All measurements were made at 20 °C and *g*-factors were referenced relative to a built-in manganese oxide marker within the resonant cavity of the instrument. Quantification of the number of unpaired electrons present in polymer **13** was done by comparing an EPR spectrum collected for a TEMPO solution of known concentration in CH_2Cl_2 that was compared to the manganese oxide marker signal as outlined above. The integration of the TEMPO signal with respect to the manganese oxide marker was compared to that of the radical polymer. By assuming one molecule of TEMPO contributes one unpaired electron, the number of unpaired electrons present in the radical polymer sample was determined.

X-ray Crystallography

Crystals of monomer **12** suitable for X-ray diffraction were grown by vapor diffusion of hexanes into a saturated CH_2Cl_2 solution at –30 °C. The sample was mounted on a MiTeGen polyimide micromount with a small amount of Paratone N oil. All X-ray measurements were made on a Nonius KappaCCD Apex2 diffractometer at a temperature of 110 K. The frame integration was performed using SAINT.[43] The resulting raw data was scaled and absorption corrected using a multi-scan averaging of symmetry equivalent data using SADABS.[44] The structure was solved by using a dual space methodology using the SHELXT program.[45] All non-hydrogen atoms were obtained from the initial solution. The hydrogen atoms were introduced at

idealized positions and the positional parameters but not the displacement parameters were allowed to refine. The structural model was fit to the data using full matrix least-squares based on F^2. The calculated structure factors included corrections for anomalous dispersion from the usual tabulation. The structure was refined using the SHELXL-2014 program from the SHELX suite of crystallographic software.[46] Graphic plots were produced using the Mercury program suite. See Table 1 and CCDC 1428231 for X-ray diffraction data collection and refinement details.

TABLE 1 Selected X-ray diffraction data collection and refinement details for monomer **12**.

Compound	**12**
Chemical Formula	$C_{27}H_{32}N_5O_5$
Formula Weight (g mol^{-1})	506.57
Crystal Dimensions (mm)	0.349 × 0.325 × 0.115
Crystal Color and Habit	Red prism
Crystal System	Triclinic
Space Group	P -1
Temperature (K)	110
a (Å)	10.063(2)
b (Å)	11.316(2)
c (Å)	12.516(2)
α (°)	100.839(4)
β (°)	112.235(5)
γ (°)	98.624(5)
V (Å^3)	1257.0(4)
Z	2
ρ (g cm^{-1})	1.338
λ (Å)	1.54178
μ (cm^{-1})	0.769
Diffractometer Type	Nonius KappaCCD Apex2
R_{merge}	0.0245
R_1[a]	0.0352
ωR_2[b]	0.0900
R_1 (all data)	0.0391
ωR_2 (all data)	0.0940
GOF[c]	1.028

[a] $R_1 = \Sigma(|F_o| - |F_c|) / \Sigma F_o$

[b] $\omega R_2 = [\Sigma(\omega(F_o^2 - F_c^2)^2) / \Sigma(\omega F_o^4)]^{½}$

[c] $GOF = [\Sigma(\omega(F_o^2 - F_c^2)^2) / (\text{No. of reflns.} - \text{No. of params.})]^{½}$

Thin-Film Preparation and Electrical Conductivity Measurements

Thin films of various thickness were prepared from polymer **13** and their electrical properties were measured. Film preparation and electrical measurements were both carried out in a glove box loaded with N_2 (Nexus II, Vacuum Atmospheres Co.) attached to an ultra-high vacuum (UHV) chamber for sample metallization and contacting. Samples can be transferred to/from this chamber from/to the glove box without any direct exposure to air. O_2 and H_2O contents in the glove box were below 3 ppm during the entire fabrication and measurement process. To prepare the thin films, the polymer was dissolved at 12.5 mg mL^{-1} in anhydrous chlorobenzene. The solution was stirred overnight at 50 °C, filtered through 0.8 μm pore size syringe filters and spun on glass substrates with pre-deposited indium tin-oxide (ITO) contacts (15 Ω/square sheet resistance, Sigma-Aldrich) using a KW-4A spin coater (Chemat Technologies Inc.) located in the glove box. ITO substrate patterning on glass was previously obtained by coating the ITO area to be retained with Kapton™ tape and etching the remaining area in a 2:1:1 H_2O:HCl:HNO_3 mixture at 55 °C.

Different spinning speeds, from 500 to 3000 rpm, were used to obtain a set of thin films at thicknesses from 50 ± 4 nm to 10 ± 4 nm, respectively. These thicknesses were measured by atomic force microscopy (AFM) from samples identical to those used for electrical measurements. In order to perform the thickness measurements, part of the substrate was masked prior to spin coating the polymer solution. The mask was then removed and samples were extracted from the glove box and analyzed in contact-mode using a Witec Alpha300S AFM microscope, from which topography profiles of the step in the correspondence of the masked area were obtained. Additional AFM profiles were recorded in the correspondence of scratches made on the polymer film using soft probes that were known not to affect the substrate. AFM

images showed that root mean squared (RMS) roughness of thin films of polymer **13** could be estimated to be about 2 nm, which was significantly less than the RMS roughness of ITO. This suggests the polymeric film is continuous with no outstanding ITO pinholes (Figure S1).

Electrical measurements were performed in a sandwich configuration in the glove box. To complete the sandwich structure, samples were transferred in the aforementioned UHV chamber directly accessible from the glove box and 100 nm thick aluminum contacts were thermally evaporated on top of the polymer films, with contact thickness measured *in situ* using a Sycom STM-2 thickness monitor. The temperature was kept below 50 °C during the entire thermal evaporation process. A first set of current voltage (I-V) characteristics of the thin films were recorded at ± 1 V using a computer automated Keithley 2400 source meter with 10 mV scan step. After this set of measurements a significantly higher voltage, $V_\circ$ = 5 V, was applied to the samples, and electrical measurements were repeated. The breakdown voltage was determined to be 8–12 V for the thinnest sample and is therefore significantly higher than any voltages used during our experiments. Consistent electrical measurements were successfully reproduced on different sets of identical samples.

1,5-di-*iso*propyl-3-(4-carboxyphenyl)-6-oxotetrazane (9)

To a refluxing solution of 2,4-di-*iso*propylcarbazide (2.00 g, 8.09 mmol) and sodium acetate (1.33 g, 16.2 mmol) in MeOH (50 mL) was added dropwise over a 3 h period, a solution of 4-carboxybenzaldehyde (1.21 g, 8.09 mmol) and sodium acetate (0.66 g, 8.1 mmol) in MeOH (50 mL). The solution was stirred at reflux overnight, removed from the heat and allowed to cool to room temperature. The reaction mixture was then acidified to pH ~ 3 using 1 M HCl, followed by the removal of MeOH *in vacuo*. The white precipitate that crashed out of the resulting aqueous solution was filtered and washed with two portions of deionized H_2O (50 mL) to give

tetrazane **9** as a white microcrystalline powder. Yield = 2.34 g, 94%. ^{1}H NMR (400.1 MHz, *d*6-DMSO): δ 13.00 (s, 1H, COO*H*), 7.97 (d, 2H, $^{3}J_{HH}$ = 6 Hz, aryl C*H*), 7.68 (d, 2H, $^{3}J_{HH}$ = 6 Hz, aryl C*H*), 5.05 (d, 2H, $^{3}J_{HH}$ = 11 Hz, N*H*), 4.50−4.43 (m, 3H, NC*H*N and C*H*Me$_2$), 1.06−1.04 (m, 12H, C*H*$_3$). ^{13}C {^{1}H}NMR (100.6 MHz, *d*6-DMSO): δ 167.0, 153.4, 141.1, 130.6, 129.3, 126.9, 72.2, 46.8, 19.6, 18.4. FT-IR (ranked intensity, assignment), KBr pellet: 3249 (13, NH), 2981 (7), 2935 (11), 2872 (12), 1694 (3, CO), 1586 (1, CO), 1423 (2), 1227 (5), 1125 (6), 1062 (8), 904 (9), 863 (10), 752 (4) cm^{-1}. Mass Spec. (EI, +ve mode): exact mass calculated for $C_{15}H_{22}N_4O_3$: 306.1692; found: 306.1688; difference: –1.3 ppm.

1,5-di-*iso*propyl-3-(4-carboxyphenyl)-6-oxoverdazyl (10)

To a deionized H_2O /THF (2:1, 45 mL) solution of 1,5-di-*iso*propyl-3-(4-carboxyphenyl)-6-oxotetrazane **9** (2.34 g, 7.64 mmol) and sodium hydroxide (0.31 g, 7.6 mmol) open to air was added sodium periodate (2.45 g, 11.5 mmol) in deionized H_2O (30 mL) dropwise over 30 min. The reaction was stirred at room temperature for 18 h and slowly turned a dark red colour. The mixture was then acidified to pH ~ 3 using 1 M HCl, followed by removal of THF *in vacuo*. The resultant dark-red precipitate was filtered and washed with two portions of deionized H_2O (50 mL) to give verdazyl **10** as a red microcrystalline powder. Yield = 2.15 g, 93%. FT-IR (ranked intensity, assignment), KBr pellet: 3434 (4, br, OH), 3198 (8), 2985 (6), 2937 (9), 1721 (3, CO), 1680 (1, CO), 1656 (2), 1612 (7), 1432 (12), 1386 (10), 1290 (11), 1219 (5) cm^{-1}. UV-vis (CH_2Cl_2): λ_{max} 419 nm (ε = 1,875 M^{-1} cm^{-1}), 405 nm (ε = 1,600 M^{-1} cm^{-1}), 270 nm (ε = 29,750 M^{-1} cm^{-1}). Mass Spec. (EI, +ve mode): exact mass calculated for $C_{15}H_{19}N_4O_3$: 303.1457; found: 303.1459; difference: +0.7 ppm.

1,5-di*iso*propyl-3-(*cis*-5-norbornene-*exo*-2,3,-dicarboxiimide)-6-oxoverdazyl (12)

To a solution of *N,N'*-dicyclohexylcarbodiimide (DCC) (0.75 g, 3.6 mmol) and 4-dimethylaminopyridine (DMAP) (0.48 g, 4.0 mmol) in dry CH_2Cl_2 (20 mL) was added 1,5-di-*iso*propyl-3-(4-carboxyphenyl)-6-oxoverdazyl **10** (1.00 g, 3.30 mmol) before the mixture was stirred for 10 min at room temperature. To this solution was added *N*-(3-hydroxylpropyl)-*cis*-5-norbornene-*exo*-2,3-dicarboximide **11** (0.73 g, 3.3 mmol) and a further 10 mL of dry CH_2Cl_2 (for rinsing). The reaction mixture was stirred for 4 h at room temperature. The solution was filtered to remove salt, which was rinsed with dry CH_2Cl_2 before the organic phases were combined and taken to dryness *in vacuo*. The resulting orange oil was purified by column chromatography [75 mL neutral alumina, hexanes/EtOAc (35:65), R_f = 0.45], and recrystallized from a hot saturated solution of hexanes to give **12** as dark-red needles. Yield = 1.18 g, 71%. FT-IR (ranked intensity, assignment), KBr pellet: 2978 (11), 2935 (12), 2877 (14), 1770 (13, CO), 1697 (1, CO), 1679 (2, CO), 1611 (10), 1386 (9), 1367 (8), 1268 (2), 1230 (5), 1174 (6), 776 (7), 705 (4) cm^{-1}. UV-vis (CH_2Cl_2): λ_{max} 418 nm (ε = 1,900 M^{-1} cm^{-1}), 403 nm (ε = 1,400 M^{-1} cm^{-1}), 268 nm (ε = 31,025 M^{-1} cm^{-1}). Mass Spec. (EI, +ve mode): exact mass calculated for $C_{27}H_{32}N_5O_5$: 506.2403; found: 506.2399; difference: −0.8 ppm. Anal. Calcd. (%) for $C_{27}H_{32}N_5O_5$: C, 64.02; H, 6.37; N, 13.82. Found: C, 63.88; H, 6.50; N, 13.65.

Representative synthesis of poly[1,5-di*iso*propyl-3-(*cis*-5-norbornene-*exo*-2,3,-dicarboxiimide)-6-oxoverdazyl] (13)

A grease-free Schlenk flask was charged with monomer **12** (0.50 g, 0.99 mmol) and degassed CH_2Cl_2 (12 mL, 3 freeze-pump-thaw cycles). The monomer solution was cooled to 0 °C in an ice bath for 10 min before a 1 mg mL^{-1} CH_2Cl_2 solution of Grubbs' 3rd generation catalyst (8.73 mL, 9.87×10^{-3} mmol) was rapidly added in one portion. The polymerization proceeded for 1 h before it was terminated with ethyl vinyl ether (2.37 mL, 24.7 mmol), and stirred for an

additional 30 min while warming to room temperature. The crude mixture was filtered through a short neutral alumina column (4 cm × 2.5 cm, CH_2Cl_2) before the solvent was removed *in vacuo*. The resultant polymer, an orange oil was dissolved in THF (10 mL) and precipitated thrice into cold hexanes (90 mL) to afford **13** as an orange powder. Yield = 0.46 g, 92%. FT-IR (ranked intensity, assignment), KBr pellet: 2975 (13), 2939 (14), 2871 (16), CO ester 1775 (15), 1698 (1, CO), 1682 (2, CO), 1611 (12), 1387 (10), 1368 (8), 1270 (3), 1228 (9), 1173 (6), 1104 (7), 1101 (5), 776 (11), 705 (4) cm^{-1}. UV-vis (CH_2Cl_2): λ_{max} 419 nm (ε = 2,050 M^{-1} cm^{-1}), 402 nm (ε = 1,475 M^{-1} cm^{-1}), 270 nm (ε = 29,900 M^{-1} cm^{-1}). GPC (THF, conventional calibration relative to polystyrene standards): M_n = 46,100 g mol^{-1}, M_w = 49,000 g mol^{-1}, $Đ$ = 1.07).

Kinetic Studies of the ROMP of Monomer 12

Catalyst Loading: Using 0.05 g of monomer **12** each, a series of five reactions were carried out according to the procedure described above. The catalyst molar feed stock ratios (monomer:catalyst) were: 20, 40, 60, 80, and 100. The polymerization times were held constant at 30 min. The degree of polymerization was measured by GPC analysis using conventional calibration relative to polystyrene standards.

Timed aliquots: A 1 mg mL^{-1} CH_2Cl_2 solution of Grubbs' 3rd generation catalyst (3.5 mL, 4.0 × 10^{-3} mmol) was rapidly added in one portion to a 42 mg mL^{-1} CH_2Cl_2 solution of monomer **12** (4.8 mL, 0.40 mmol) and the mixture was stirred at 0 °C. Six samples were taken at 150 s intervals and added into separate reaction flasks containing ethyl vinyl ether (0.94 mL, 9.9 mmol) to terminate polymerization. The number average molecular weights (M_n) were measured by GPC analysis using conventional calibration relative to polystyrene standards.

RESULTS AND DISCUSSION

Synthesis

The synthesis of monomer **12** (Scheme 1) began with the condensation reaction between bis-hydrazide×2HCl salt **8** and 4-formylbenzoic acid to afford tetrazane **9** as a white powder in 94% yield (Figure S2 and S3). Tetrazane **9** was then oxidized in THF/deionized H_2O solution using sodium periodate to yield 6-oxoverdazyl **10** as an orange powder (93%). The reaction was monitored by FT-IR spectroscopy where the disappearance of the NH stretch at 3249 cm^{-1} was observed (Figure S4). Verdazyl **10** was then coupled to *N*-(3-hydroxylpropyl)-*cis*-5-norbornene-*exo*-2,3-dicarboximide **11** in the presence of DCC and DMAP to afford monomer **12** as dark-red crystals in 71% yield. The propyl-substituted *cis*-5-norbornene-*exo*-2,3-dicarboximide polymerizable group was chosen based on previous reports by Tang and co-workers describing the successful ROMP of monomers bearing redox-active cobaltocenium moieties.[42]

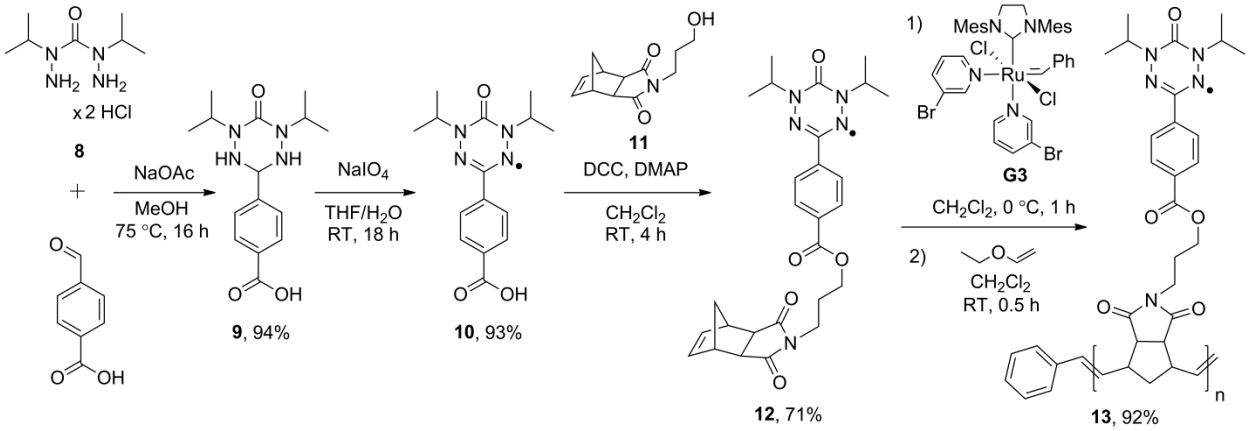

SCHEME 1 Synthesis of 6-oxoverdazyl monomer **12** and polymer **13**.

X-ray diffraction studies of single crystals of monomer **12** afforded a solid-state structure (Figure 2 and Table 1). The bond lengths of N1-N2 1.3558(15) and N3-N4 1.3595(15) Å are intermediate between single and double N-N bonds.[47] Similarly, the N2-C1 1.3319(16) and N4-C1 1.3315(16) Å bond lengths fall between those expected for single and double N-C bonds,[47]

confirming the delocalized nature of the bonding in the planar verdazyl radical. The dihedral angle between the verdazyl plane (N1-N2-C1-N4-N3-C2) and the plane defined by the phenyl ring (C9–C14) was found to be 6.13°. Furthermore, the bond length of C24-C25 of 1.318(2) Å is consistent with the preservation of the alkene in the norbornene ring. The structural metrics observed for verdazyl monomer **12** are consistent with those of other 6-oxoverdazyl radicals.[34,48-52]

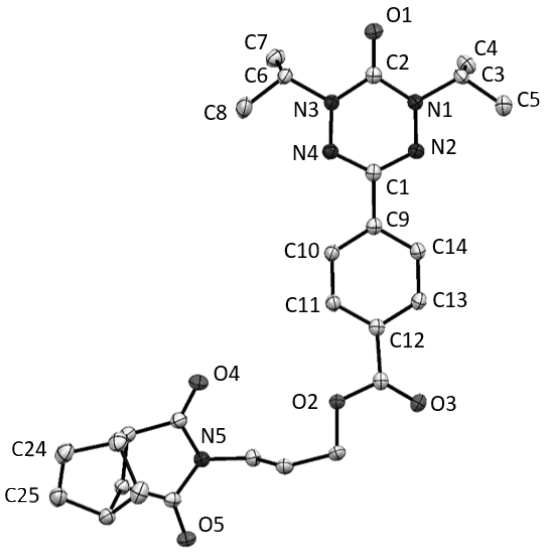

FIGURE 2 Solid-state structure of monomer **12**. Anisotropic displacement ellipsoids are shown at 50% probability and hydrogen atoms have been omitted for clarity. Selected bond lengths (Å): N1-N2 1.3558(15), N3-N4 1.3595(15), N1-C2 1.3819(16), N2-C1 1.3319(16), N3-C2 1.3802(16), N4-C1 1.3315(16), C24-C25 1.318(2). Selected bond angles (deg): N1-N2-C1 115.00(10), N3-N4-C1 114.96(10), N1-C2-N3 114.35(11), N2-C1-N4 127.20(11).

With monomer **12** in hand, we began to explore its ROMP behavior. In a representative reaction, polymerization was initiated by the rapid introduction of a solution of Grubbs' 3rd generation catalyst (G3) to a stirring solution of monomer **12** in dry and degassed CH_2Cl_2 at 0 °C with a feed molar ratio of 100 (monomer:catalyst = 100:1). Reaction progress was monitored by gel permeation chromatography (GPC), confirming the reaction was near completion after approximately 15 min. Nonetheless, the solution was stirred for an additional 45 min to ensure

complete monomer conversion before a large excess of ethyl vinyl ether (EVE) was added to terminate the polymerization. The reaction mixture was passed through a plug of neutral alumina to remove residual catalyst. Subsequent precipitations from THF into cold hexanes, followed by centrifugation afforded polymer **13** as an orange powder in 92% yield. Figure 3a shows the GPC trace (typical) obtained for polymer **13** after purification [number average molecular weight (M_n) = 46,100 g mol^{-1}, weight average molecular weight (M_w) = 49,300 g mol^{-1}, dispersity ($Đ$) = 1.07]. Our best results were obtained when CH_2Cl_2 was employed as a solvent, while Nishide and co-workers have recently noted improved results when acetone was employed as solvent for the ROMP of a related bis nitroxide monomer.[26]

It is worth noting that during our investigations of the ROMP of monomer **12**, approximately 20% of our reactions yielded polymer samples that contained a high molecular weight shoulder in their GPC chromatograms (*e.g.*, Figure 3b, M_n = 51,100 g mol^{-1}, M_w = 57,750 g mol^{-1}, $Đ$ =1.13). Based on the inconsistent appearance of this shoulder in our GPC data, we assume that the high molecular weight species are generated via chain coupling or related reactions during the termination step. The origin of the coupling remains unclear, however, molecular oxygen inadvertently introduced when EVE was introduced to the reaction flask via syringe may play a role in the observed reactivity.

We performed two separate experiments designed to further probe the ROMP of monomer **12**. Unfortunately, the scope of our studies were limited due to the paramagnetic nature of polymer **13**, which precluded the use of integration data obtained from ^{1}H NMR spectroscopy for the determination of the number average degree of polymerization (DP_n) and monomer consumption as a function of time. The first study involved ROMP of monomer **12** at five different molar feedstock ratios (Figure 3c). As expected, the values of DP_n determined by GPC

analysis increased significantly as the molar feedstock ratios were increased from 20 to 100. However, when high molecular weight polymers were targeted, we observed a deviation from ideal behavior, and lower than expected values of DP_n. This observation is indicative of well-behaved, but not formally living polymerization ROMP. A second study was performed, where a single ROMP reaction (monomer:catalyst 100:1) was studied at time intervals of 150 s (Figure 3d). The molecular weight of the isolated polymers increased in a non-linear fashion as a function of time due to a decrease in monomer concentration as the reaction proceeded. Again, this trend was consistent with a well-behaved ROMP reaction involving limited side reactions.

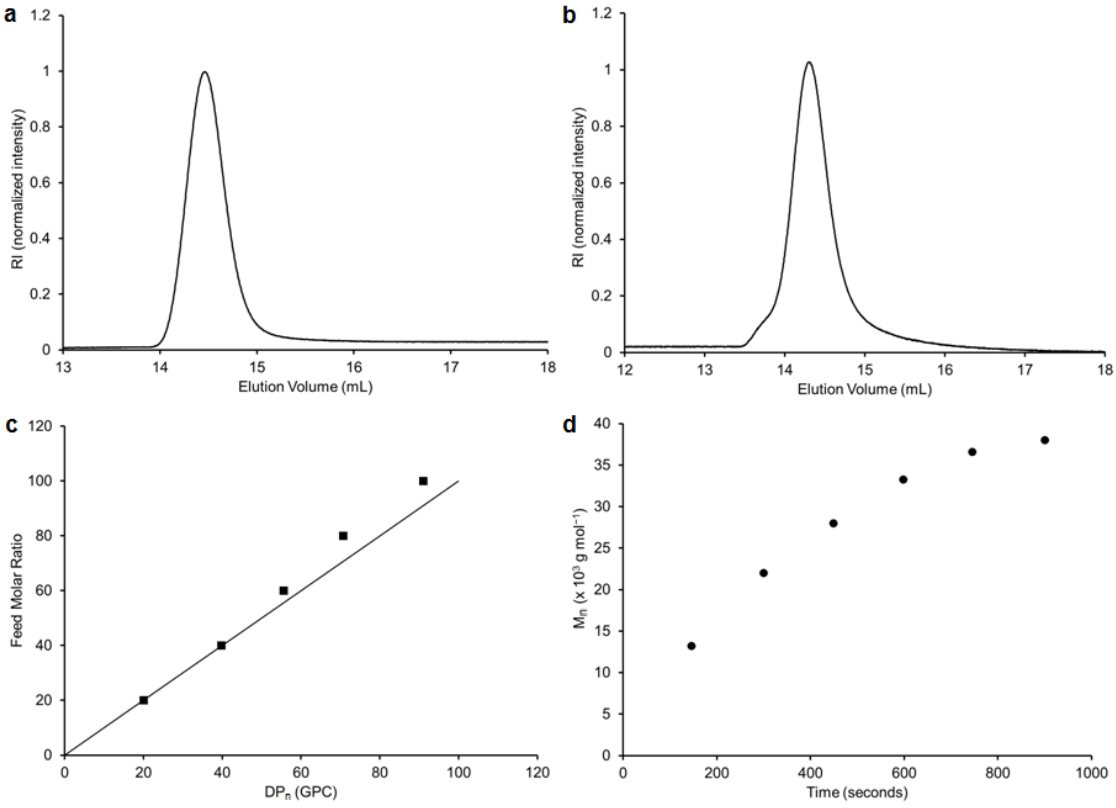

FIGURE 3 Representative GPC traces for (a) a typical sample of polymer **13** (M_n = 46,100 g mol^{-1}, M_w = 49,300 g mol^{-1}, $Đ$ = 1.07) and (b) a GPC trace for a polymer containing a minor fraction of high molecular weight polymer **13** (M_n = 51,100 g mol^{-1}, M_w = 57,750 g mol^{-1}, $Đ$ = 1.13). (c) Relationship of feed molar ratio and DP_n determined by GPC. The black line represents the theoretical relationship between DP_n and feed molar ratio. (d) Molecular weight (M_n) as a function of reaction time.

Polymer Characterization

Thermal gravimetric analysis (TGA) revealed that polymer **13** was thermally stable up to a temperature of 190 °C, where rapid degradation occurred in three steps (Figure S5). The first step (190–290 °C) involved a mass loss of 13%, the second (290–430 °C) 35%, and the third (430–800 °C) 40%, to give an overall char yield of 12%. Differential scanning calorimetry (DSC) studies of polymer **13** revealed a T_g of 152 °C (Figure S6).

To confirm the presence of 6-oxoverdazyl radicals in the polymer, careful comparison of the spectroscopic and electrochemical properties of monomer **12** and polymer **13** were made. The FT-IR spectra of monomer **12** showed characteristic carbonyl peaks at 1679, 1697, 1770 cm^{-1} similar to the carbonyl peaks at 1682, 1698, and 1775 cm^{-1} of polymer **13** (Figure S7). Moreover, when we compared the UV-vis absorption spectra of monomer **12** and polymer **13** between 350 and 475 nm, we found that they were in very close agreement (Figure 4). Based on the IR and UV-vis absorption spectra, we conclude that nearly 100% of the repeating units in polymer **13** contain a 6-oxoverdazyl moiety, indicating that the ROMP reaction employed is indeed tolerant of such radicals.

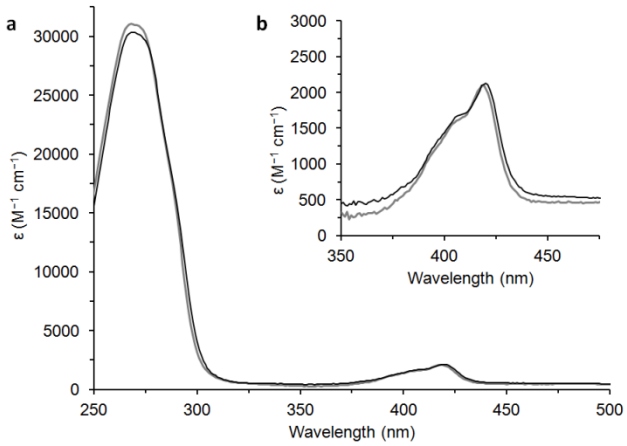

FIGURE 4 (a) UV-vis absorption spectra acquired for CH_2Cl_2 solutions of monomer **12** (grey line) and polymer **13** (black line). (b) Magnified spectra from 350 to 475 nm.

In order to further support these findings, electron paramagnetic resonance (EPR) spectroscopy was performed to quantitatively determine the number of unpaired 6-oxoverdazyl units present in polymer **13**. This experiment showed that *ca.* 94% of the repeating units in the polymer contain an unpaired electron, supporting our IR and UV-vis absorption spectroscopy-based claims discussed above. An EPR spectrum of monomer **12** was also obtained and compared to the spectrum of polymer **13** (Figure 5). The spectrum of monomer **12** showed a typical pattern for 1,5-substituted 6-oxoverdazyls,[41] with the radical coupling to two unique pairs of nitrogen atoms and the CH protons of the isopropyl groups [simulation data (Figure S8): g = 2.0045, line width = 0.089 mT, $a_{N1,3}$ = 0.529 mT, $a_{N2,4}$ = 0.640 mT, a_H = 0.140 mT]. The isotropic EPR spectrum of polymer **13** (g = 2.0043) was very broad and essentially featureless, as would be expected for a polymer containing stable radicals in random orientations and close proximity.

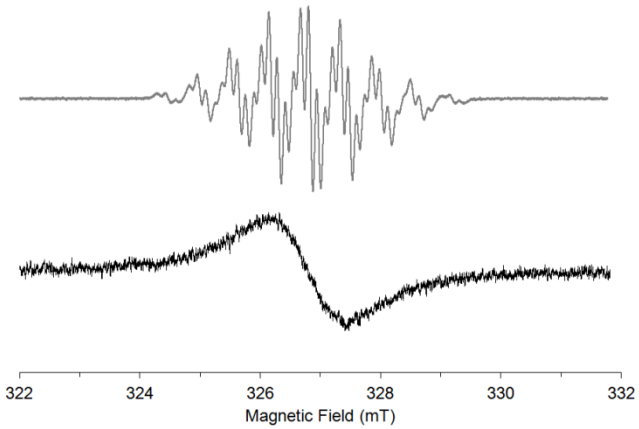

FIGURE 5 Experimental EPR spectra of 6-oxoverdazyl monomer **12** (grey line, g = 2.0045) and polymer **13** (black line, g = 2.0043). Simulation of the spectrum of monomer **12** yielded the following parameters: line width = 0.089 mT, $a_{N1,3}$ = 0.529 mT, $a_{N2,4}$ = 0.640 mT, a_H = 0.140 mT (Figure S8).

The electrochemical properties of monomer **12** and polymer **13** were studied using cyclic voltammetry (CV) in a CH_2Cl_2/MeCN (1:1) solvent mixture (Figure 6, Table 2). 6-Oxoverdazyl monomer **12** was reversibly oxidized and reduced at half-wave oxidation ($E_{1/2,ox}$) and reduction ($E_{1/2,red}$) potentials of 0.24 and −1.36 V relative to the ferrocene/ferrocenium redox couple, respectively. Similarly, the CV of polymer **13** showed oxidation and reduction wave potentials at 0.25 V and −1.35 V, respectively. The current response for the polymer was lower than expected and the oxidation/reduction waves broadened as a result of a loss of diffusion control at the electrode interface, a commonly observed phenomenon for redox-active polymers.

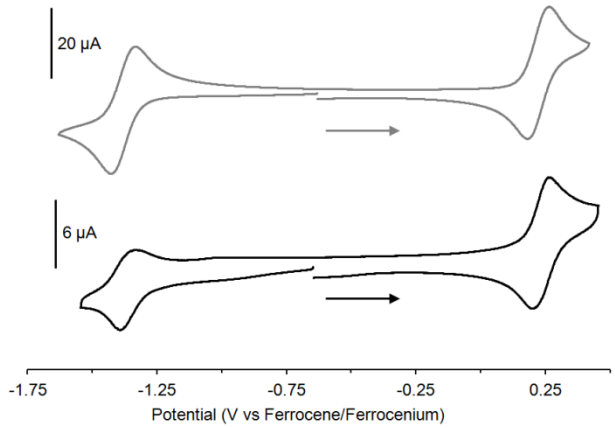

FIGURE 6 Cyclic voltammograms of 6-oxoverdazyl monomer **12** (grey line) and polymer **13** (black line) recorded at a scan rate of 100 mV s^{-1} in CH_2Cl_2/MeCN (1:1) solution containing 1 mM analyte and 0.1 M nBu$_4$NPF$_6$ as supporting electrolyte.

TABLE 2 Electrochemical data for 6-oxoverdazyl monomer **12** and polymer **13**.

Compound	$E_{1/2,ox}$ (V vs. Fc/Fc^+)	$E_{1/2,red}$ (V vs. Fc/Fc^+)
12	0.24	−1.36
13	0.25	−1.35

Electrical Properties of Thin Films of Polymer 13

Based on the spectroscopic and electrochemical studies described above, we concluded that polymer **13** may have interesting and potentially unique thin-film properties. To this end, we investigated the electrical properties of thin solid films of this polymer, from approximately 10 nm to 50 nm in thickness, by using a sandwich architecture. Thin polymeric films may have very peculiar morphological and structural properties[53] as a consequence of the preferential alignment of the polymeric chains with respect to the substrate. Specifically, the alignment may be strongly dependent on the thickness, which may sometimes lead to non-ohmic conductivity mechanisms and thickness-dependent resistivity in ultrathin polymeric films.[53]

Figure 7a illustrates the configuration we used to measure the I-V characteristics of our films before and after the films were pretreated at high voltage ($V_\circ$ = 5 V). In both cases, the film resistivity (ρ) was inferred from the I-V characteristics through the relationship

$$\rho = \frac{R \cdot A}{d} \tag{1}$$

where A is the area of the region in which the top and bottom contacts overlap, d is the film thickness and $R = V/I$ is the thin film resistance, obtained from the slope of the I-V characteristics in the proximity of the origin. The I-V curves recorded from our films of polymer **13** are reported in Figure 7b and 7c for measurements recorded after and before 5 V film treatment, respectively. In ohmic systems ρ is an inherent property of the material, independent of the thickness of the thin film that is being considered. After 5 V treatment, all films were electrically ohmic and exhibit a relatively high conductivity, with linear I-V characteristics in the entire ± 1 V range as can be observed in Figure 7b. The extracted resistivity value ($\rho \approx 1.7 \times 10^4$ Ω·m, Figure 7d) is thickness independent, as can be expected from ohmic systems. This value favorably compares with poly(2,2,6,6-tetramethylpiperidinyloxy methacrylate) **1** ($\rho \approx 1 \times 10^4$ Ω·m),[15] the most widely studied stable radical polymer that has also shown defect-dependent thin-film properties.[16] In contrast, Figure 7d also shows that these films are significantly more insulating before the high voltage treatment at 5 V. They revert to such a low-conductivity state after the effects of high-voltage treatment vanish, typically in 20–200 h.

Although a more complete understanding of the electrical properties of our films is beyond the scope of this paper and will be the subject of future reports, it is noteworthy that the I-V characteristics before high-voltage treatment of our films are typically non-ohmic, as can be

inferred from Figure 7c. As a consequence of non-ohmicity, the resistivity inferred from eq. (1) strongly increases as the thickness of the films decreases and could not be measured with our equipment at thicknesses below 20 nm. This suggests that ρ should be higher than 10^{12} Ω·m below this thickness value and, therefore, it may be approximately comparable with that of glass ($\rho \approx 10^{12}$–10^{14} Ω·m).[54] It can be phenomenologically observed that the I-V curves shown in Figure 7c can be fitted using a Poole-Frenkel model for non-ohmic transport via localized trapped charges,[55] in which the current is related to the voltage by the following relationship:

$$I = \frac{A}{\rho_o d} V \exp\left\{ \frac{-q\Delta\varphi + q^{3/2}\pi^{-1/2}\left[V/(\varepsilon_m d)\right]^{1/2}}{k_B T} \right\} \quad (2)$$

where $\rho_\circ$ corresponds to the polymer resistivity in the absence of traps, q is the electron charge, $\Delta\varphi$ is the voltage barrier electrons must cross at low voltage to hop from one charged trap to another, ε_m is the dielectric permittivity of the polymer relative to vacuum, and $k_B T = 0.025$ eV at room temperature.

While the high-conductivity state observed in Figure 7b can be attributed to extended-state transport via free electrons, the low-conductivity, Poole-Frenkel-like transport mechanism observed in Figure 7c can be assigned to hopping between localized states situated at specific charged monomers along a polymer filament. The hopping conditions may be strongly dependent on the degree of alignment of the polymer filaments along the substrate, in analogy to what previously observed in polythiophenes.[53] Specifically, if all of the polymer chains are aligned parallel to the substrate, hopping along the z-direction must occur through localized states situated on different polymer chains, thus explaining why the thinnest films, presumably

containing polymer filaments more aligned along the substrate, are also more electrically insulating.

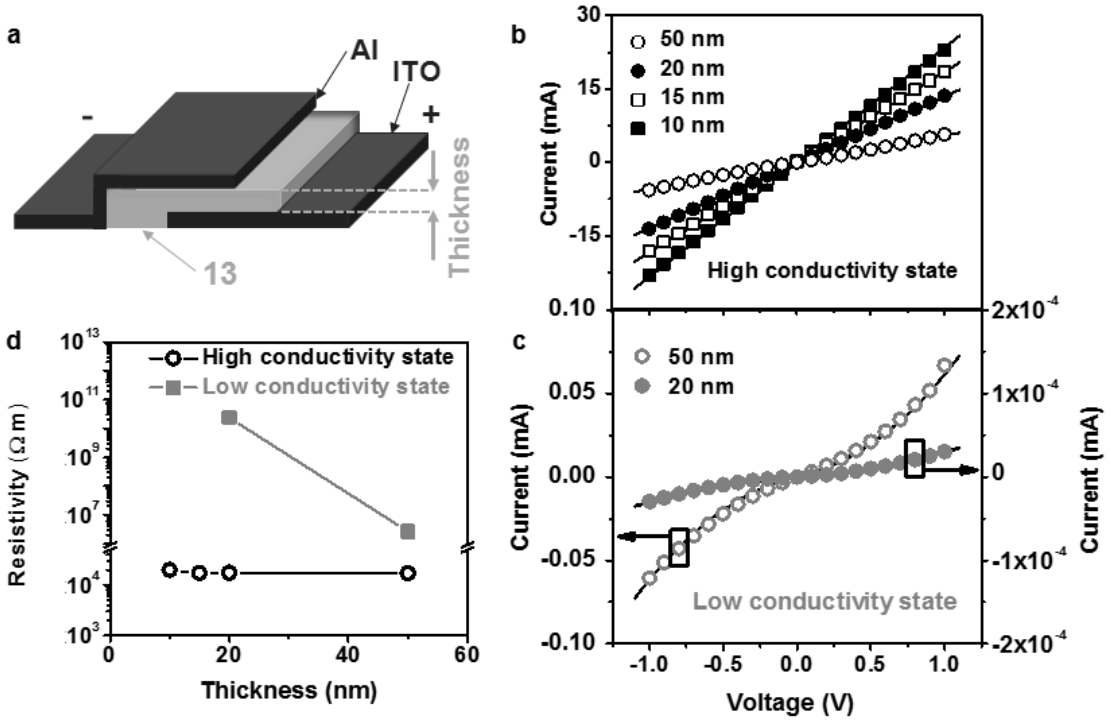

FIGURE 7 (a) Sandwich-type configuration for measuring the I-V characteristics of polymer **13** thin films, showing bistable electrical transport. (b) I-V curves of thin films at four different thicknesses in high conductivity state, which were fitted with straight lines to demonstrate ohmic transport and (c) I-V curves of thin films in low conductivity state showing non-ohmic, Poole-Frenkel like, behavior. Solid line fits were performed using eq. (2). (d) Film resistivity values obtained from the low-voltage portions of I-V curves. Resistivity is thickness-independent in the high conductivity state, while it dramatically increases at decreasing thickness in the low-conductivity state, possibly due to preferential alignment of polymer filaments along the substrate.

The switchable conductor-insulator transitions in thin films of polymer **13** and their relationship with the redox processes in this material requires further investigations. However, the observation of Poole-Frenkel type transport in the low conductivity state leads us to tentatively suggest that such state corresponds to a situation in which only a few repeating units

in a polymer chain are charged, while most of them are in a neutral state. At sufficiently high voltage (*i.e.*, $V \geq V_o \approx 5$ V) charges may directly tunnel from the electrodes into some of the neutral repeating units, charging them either positively or negatively. When a sufficient concentration of charged repeating units is reached in a thin film, a percolating pathway may be established between such repeating units, leading to switching to the high conductivity state, dominated by transport between extended electronic states. This conductor-insulator transition makes polymer **13** uniquely positioned for several applications in bistable electronics and will be the subject of future reports.

CONCLUSION

As a result of this work, we have demonstrated that ROMP using Grubbs' 3rd generation catalyst can be used to produce 6-oxoverdazyl polymers with up to *ca.* 100 repeating units, narrow molecular weight distributions ($Đ < 1.2$), and high radical content (*ca.* 94%). A representative sample of the 6-oxoverdazyl polymers produced was thermally stable up to a temperature of 190 °C and had a glass transition temperature of 152 °C. Comparison of the same polymer, which is stable towards air and moisture, to the monomer employed using several spectroscopic techniques, including IR, UV-vis absorption, and EPR spectroscopy and cyclic voltammetry confirmed the identity and properties of the pendant 6-oxoverdazyl groups were maintained after ROMP. The redox properties of the polymers described led us to explore their thin-film electrical transport properties, revealing a significant decrease in sheet resistance from 240 Ω to 26 MΩ upon application of a potential, $V_\circ = 5$ V. Our future work in this area will include expansion of the ROMP methods described to include other stable radical monomers and a detailed description of the electrical transport mechanism in 6-oxoverdazyl polymers in the solid state.

ACKNOWLEDGEMENTS

We would like to thank the University of Western Ontario, the Natural Science and Engineering Research Council (NSERC) of Canada (J.B.G. and G.F.: DG, 435675 and 506004 and J.A.P: postgraduate scholarships), and the Ontario Ministry of Research and Innovation (J.B.G.: ERA, ER14-10-147) for funding this work. V.Y.'s visit to the University of Western Ontario was supported by an Ontario-Maharastra/Goa (OMG) Scholarship under the OMG International Student Exchange Program. The authors would also like to thank Ms. Stephanie M. Barbon (EPR spectroscopy and X-ray crystallography) and Dr. Reg Bauld (EPR spectroscopy) for their contributions to this work. Finally, we thank Profs. E.R. Gillies and P.J. Ragogna for access to instrumentation in their labs.

REFERENCES AND NOTES

1 G. Meller, T. Grasser, Organic Electronics; Springer: Berlin, 2010.

2 R. G. Hicks, Stable radicals: fundamentals and applied aspects of odd-electron compounds; Wiley: Chichester, UK, 2010.

3 K. Oyaizu, H. Nishide, *Adv. Mater.* **2009**, *21*, 2339−2344.

4 T. Janoschka, M. D. Hager, U. S. Schubert, *Adv. Mater.* **2012**, *24*, 6397−6409.

5 E. P. Tomlinson, M. E. Hay, B. W. Boudouris, *Macromolecules* **2014**, *47*, 6145−6158.

6 T. Janoselika, N. Martin, U. Martin, C. Friebe, S. Morgenstern, H. Hiller, M. D. Hager, U. S. Schubert, *Nature* **2015**, *527*, 78−81.

7 W. Choi, S. Ohtani, K. Oyaizu, H. Nishide, K. E. Geckeler, *Adv. Mater.* **2011**, *23*, 4440−4443.

8 W. Choi, S. Endo, K. Oyaizu, H. Nishide, K. E. Geckeler, *J. Mater. Chem. A* **2013**, *1*, 2999−3003.

9 T. Sukegawa, K. Sato, K. Oyaizu, H. Nishide, *RSC Adv.* **2015**, *5*, 15448−15452.

10 A. Aqil, A. Vlad, M.-L. Piedboeuf, M. Aqil, N. Job, S. Melinte, C. Detrembleur, C. Jérôme, *Chem. Commun.* **2015**, *51*, 9301−9304.

11 N. M. Gallagher, A. Olankitwanit, A. Rajca, *J. Org. Chem.* **2015**, *80*, 1291−1298.

12 K. Saito, K. Hirose, T. Okayasu, H. Nishide, M. T. W. Hearn, *RSC Adv.* **2013**, *3*, 9752−9756.

13 S. Liu, X. Chu, H. Wang, F. Zhao, E. Tang, *Ind. Eng. Chem. Res.* **2015**, *54*, 5475−5480.

14 T. K. Kunz, M. O. Wolf, *Polym. Chem.* **2011**, *2*, 640-644.

15 L. Rostro, A. G. Baradwaj, B. W. Boudouris, *ACS Appl. Mater. Interfaces* **2013**, *5*, 9896-9901.

16 L. Rostro, S. H. Wong, B. W. Boudouris, *Macromolecules* **2014**, *47*, 3713−3719.

17 Y. Yonekuta, K. Susuki, K. Oyaizu, K. Honda, H. Nishide, *J. Am. Chem. Soc.* **2007**, *129*, 14128−14129.

18 Y. Yonekuta, K. Honda, H. Nishide, *Polym. Adv. Technol.* **2008**, *19*, 281−284.

19 T. Suga, K. Aoki, H. Nishide, *ACS Macro Lett.* **2015**, *4*, 892−896.

20 M. Suguro, S. Iwasa, K. Nakahara, *Macromol. Rapid Commun.* **2008**, *29*, 1635−1639.

21 J. Qu, T. Katsumata, M. Satoh, J. Wada, T. Masuda, *Polymer* **2009**, *50*, 391−396.

22 Y.-H. Wang, M.-K. Hung, C.-H. Lin, H.-C. Lin, J.-T. Lee, *Chem. Commun.* **2011**, *47*, 1249−1251.

23 T. K. Kunz, M. O. Wolf, *Polym. Chem.* **2011**, *2*, 640−644.

24 M.-K. Hung, Y.-H. Wang, C.-H. Lin, H.-C. Lin, J.-T. Lee, *J. Mater. Chem.* **2012**, *22*, 1570−1577.

25 T. Janoschka, A. Teichler, A. Krieg, M. D. Hager, U. S. Schubert, *J. Polym. Sci., Part A: Polym. Chem.* **2012**, *50*, 1394−1407.

26 T. Suga, M. Sakata, K. Aoki, H. Nishide, *ACS Macro Lett.* **2014**, *3*, 703−707.

27 B. Ernould, M. Devos, J.-P. Bourgeois, J. Rolland, A. Vlad, J.-F. Gohy, *J. Mater. Chem. A* **2015**, *3*, 8832−8839.

28 T. W. Kemper, R. E. Larsen, T. Gennett, *J. Phys. Chem. C* **2015**, *119*, 21369−21375.

29 T. Suga, S. Sugita, H. Ohshiro, K. Oyaizu, H. Nishide, *Adv. Mater.* **2011**, *23*, 751−754.

30 J. Qu, T. Fujii, T. Katsumata, Y. Suzuki, M. Shiotsuki, F. Sanda, M. Satoh, J. Wada, T. Masuda, *J. Polym. Sci., Part A: Polym. Chem.* **2007**, *45*, 5431−5445.

31 P. Nesvadba, L. Bugnon, P. Maire, P. Novák, *Chem. Mater.* **2010**, *22*, 783−788.

32 T. Suga, Y.-J. Pu, S. Kasatori, H. Nishide, *Macromolecules* **2007**, *40*, 3167−3173.

33 T. Suga, H. Ohshiro, S. Sugita, K. Oyaizu, H. Nishide, *Adv. Mater.* **2009**, *21*, 1627−1630.

34 J. T. Price, J. A. Paquette, C. S. Harrison, R. Bauld, G. Fanchini, J. B. Gilroy, *Polym. Chem.* **2014**, *5*, 5223−5226.

35 J. B. Gilroy, S. D. J. McKinnon, B. D. Koivisto, R. G. Hicks, *Org. Lett.* **2007**, *9*, 4837−4840.

36 Y. Takahashi, N. Hayashi, K. Oyaizu, K. Honda, H. Nishide, *Polym. J.* **2008**, *40*, 763−767.

37 T. Katsumata, J. Qu, M. Shiotsuki, M. Satoh, J. Wada, J. Igarashi, K. Mizoguchi, T. Masuda, *Macromolecules* **2008**, *41*, 1175−1183.

38 K. Oyaizu, Y. Ando, H. Konishi, H. Nishide, *J. Am. Chem. Soc.* **2008**, *130*, 14459−14461.

39 T. Sukegawa, H. Omata, I. Masuko, K. Oyaizu, H. Nishide, *ACS Macro Lett.* **2014**, *3*, 240−243.

40 T. Jähnert, B. Häupler, T. Janoschka, M. D. Hager, U. S. Schubert, *Macromol. Rapid Commun.* **2014**, *35*, 882−887.

41 E. C. Paré, D. J. R. Brook, A. Brieger, M. Badik, M. Schinke, *Org. Biomol. Chem.* **2005**, *3*, 4258−4261.

42 L. Ren, J. Zhang, X. Bai, C. G. Hardy, K. D. Shimizu, C. Tang, *Chem. Sci.* **2012**, *3*, 580−583.

43 Bruker-AXS, SAINT version 2013.8, **2013**, Bruker-AXS, Madison, WI 53711, USA.

44 Bruker-AXS, SADABS version 2012.1, **2012**, Bruker-AXS, Madison, WI 53711, USA.

45 G. M. Sheldrick, *Acta Crystallogr., Sect. C: Struct. Chem.* **2015**, *71*, 3−8.

46 G. M. Sheldrick, *Acta Crystallogr., Sect. A: Found. Adv.* **2015**, *71*, 3−8.

47 CRC Handbook of Chemistry and Physics; CRC Press: Boca Ranton, FL, 2013.

48 J. B. Gilroy, B. D. Koivisto, R. McDonald, M. J. Ferguson, R. G. Hicks, *J. Mater. Chem.* **2006**, *16*, 2618−2624.

49 D. J. R. Brook, G. T. Yee, *J. Org. Chem.* **2006**, *71*, 4889−4895.

50 J. B. Gilroy, S. D. J. McKinnon, P. Kennepohl, M. S. Zsombor, M. J. Ferguson, L. K. Thompson, R. G. Hicks, *J. Org. Chem.* **2007**, *72*, 8062−8069.

51 V. Chemistruck, D. Chambers, D. J. R. Brook, *J. Org. Chem.* **2009**, *74*, 1850−1857.

52 K. J. Anderson, J. B. Gilroy, B. O. Patrick, R. McDonald, M. J. Ferguson, R. G. Hicks, *Inorg. Chim. Acta* **2011**, *374*, 480−488.

53 A. M. Nardes, M. Kemerink, R. A. J. Janssen, J. A. M. Bastiaansen, N. M. M. Kiggen, B. M. W. Langeveld, A. J. J. M. van Breemen, M. M. de Kok, *Adv. Mater.* **2007**, *19*, 1196−1200.

54 D. J. Griffiths, Introduction to Electrodynamics; Prentice Hall: Upper Saddle River, New Jersey, 1999, 286.

55 S. M. Sze, Physics of Semiconductor Devices; Wiley: New York, 1998, Sect. 7.4.4.

Supporting Information

Synthesis, Characterization, and Thin-film Properties of 6-Oxoverdazyl Polymers Prepared by Ring-Opening Metathesis Polymerization

Joseph A. Paquette,[1,2] Sabastine Ezugwu,[2,3] Vishal Yadav, [2,3] Giovanni Fanchini,*[1,2,3] and Joe B. Gilroy*[1,2]

[1]*Department of Chemistry and* [2]*The Centre for Advanced Materials and Biomaterials Research (CAMBR), The University of Western Ontario, London, ON, Canada, N6A 5B7.* [3]*Department of Physics and Astronomy, The University of Western Ontario, London. ON, Canada, N6A 3K7.*

E-mail: gfanchin@uwo.ca, joe.gilroy@uwo.ca

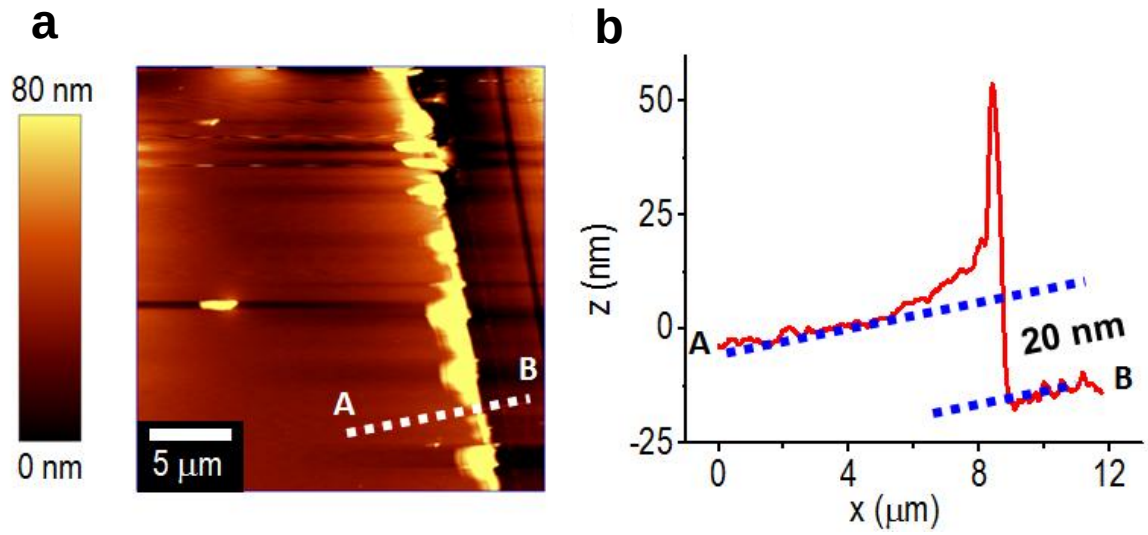

FIGURE S1 (a) Atomic Force Microscopy (AFM) image of a 20 nm thin film of polymer **13** (left side of the image) and indium-tin oxide (ITO) substrate (right side of the image). (b) Z-axis profile of the "step" at the edge of polymer **13** used to determine the thin film thickness. From the right side of the profile, root mean squared (RMS) roughness of ITO could be estimated to be about 4 nm, much less than the polymer thickness, which is about 20 nm with an RMS roughness of about 2 nm, significantly less than the RMS roughness of ITO. This suggests the polymeric film is continuous with no outstanding ITO pinholes.

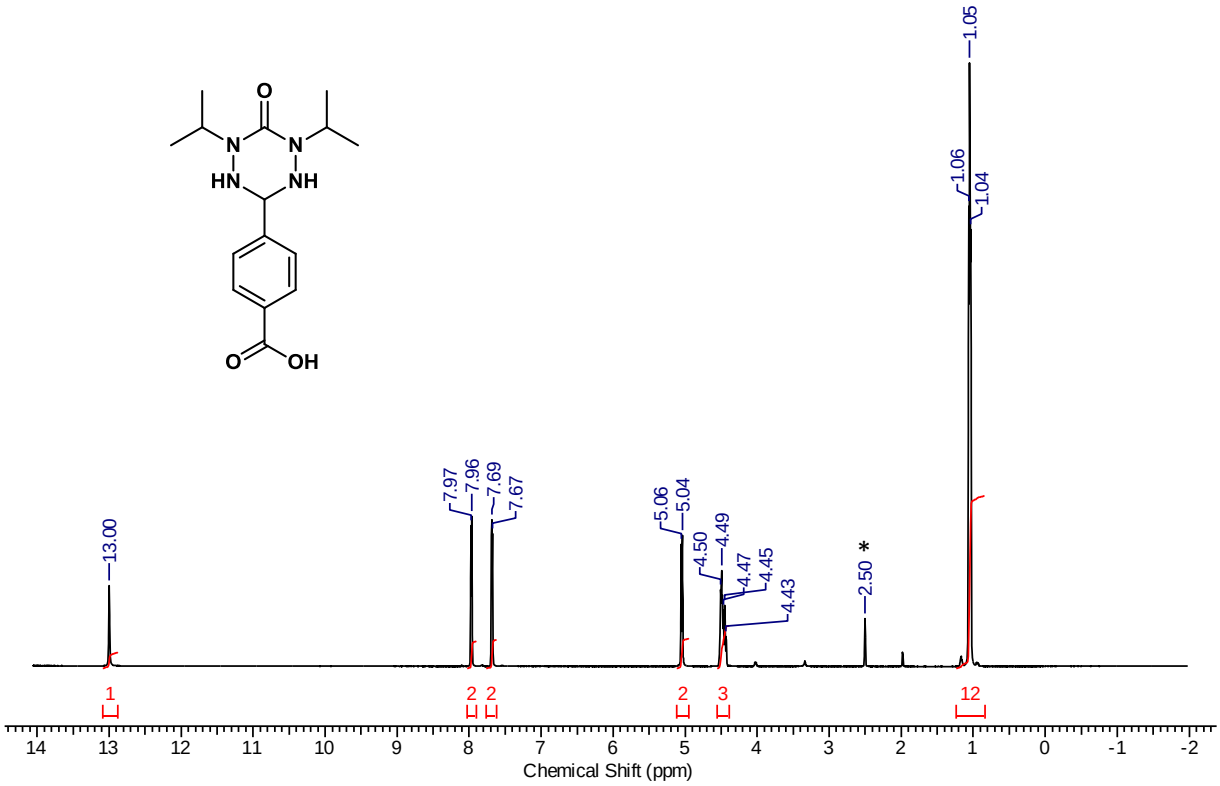

FIGURE S2 ^{1}H NMR spectrum of tetrazane **9** in d_6-DMSO. The asterisk denotes residual CD_3SOCD_2H.

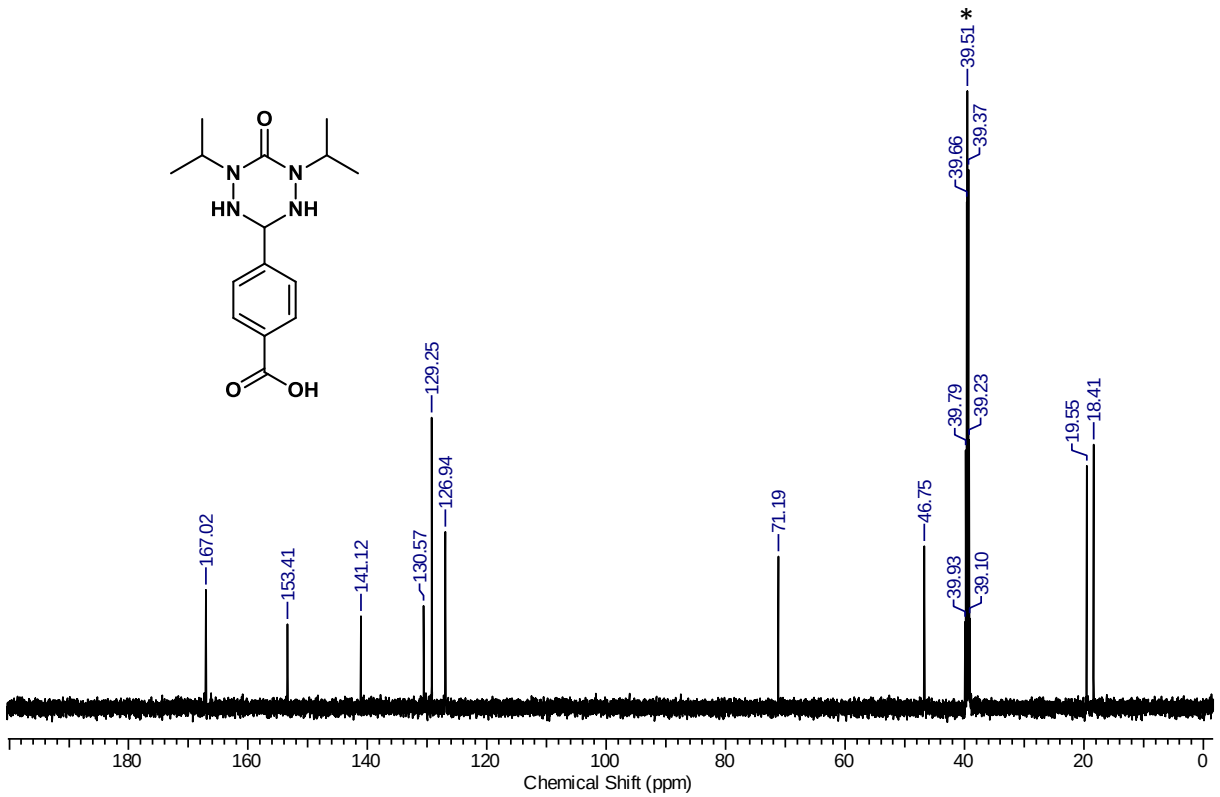

FIGURE S3 ^{13}C {^{1}H} NMR spectrum of tetrazane **9** in d_6-DMSO. The asterisk denotes d_6-DMSO.

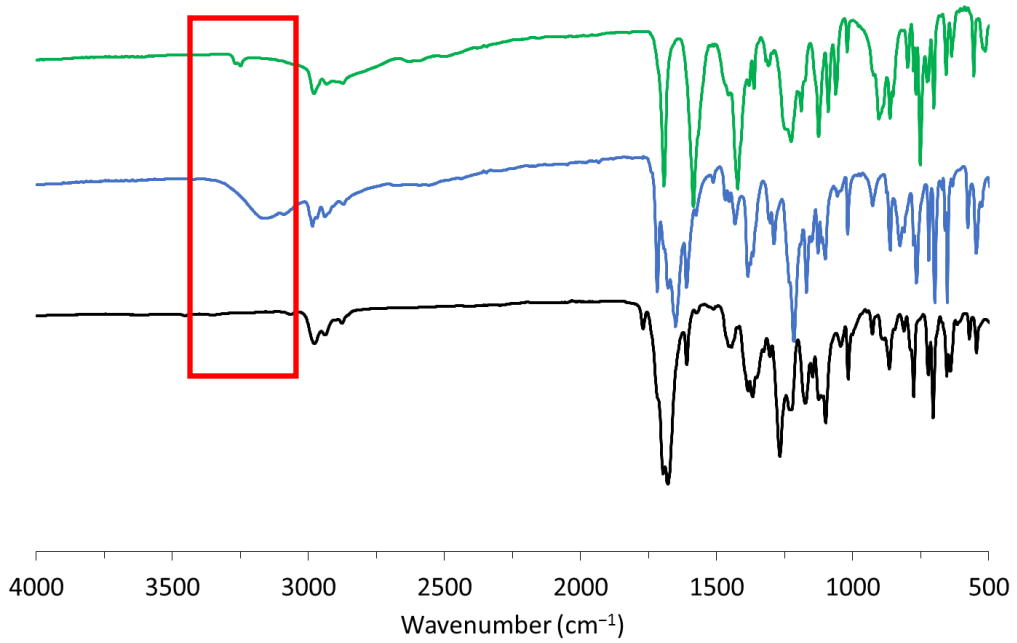

FIGURE S4 FT-IR spectra of tetrazane **9** (green line), 6-oxoverdazyl **10** (blue line), and monomer **12** (black line). Baselines have been offset for ease of comparison. Note the disappearance of the stretch at 3249 cm^{-1} upon oxidation of tetrazane **9** to verdazyl **10**, and the disappearance of the broad COOH stretch at 3434 cm^{-1} after the DCC coupling reaction (**10** → **12**).

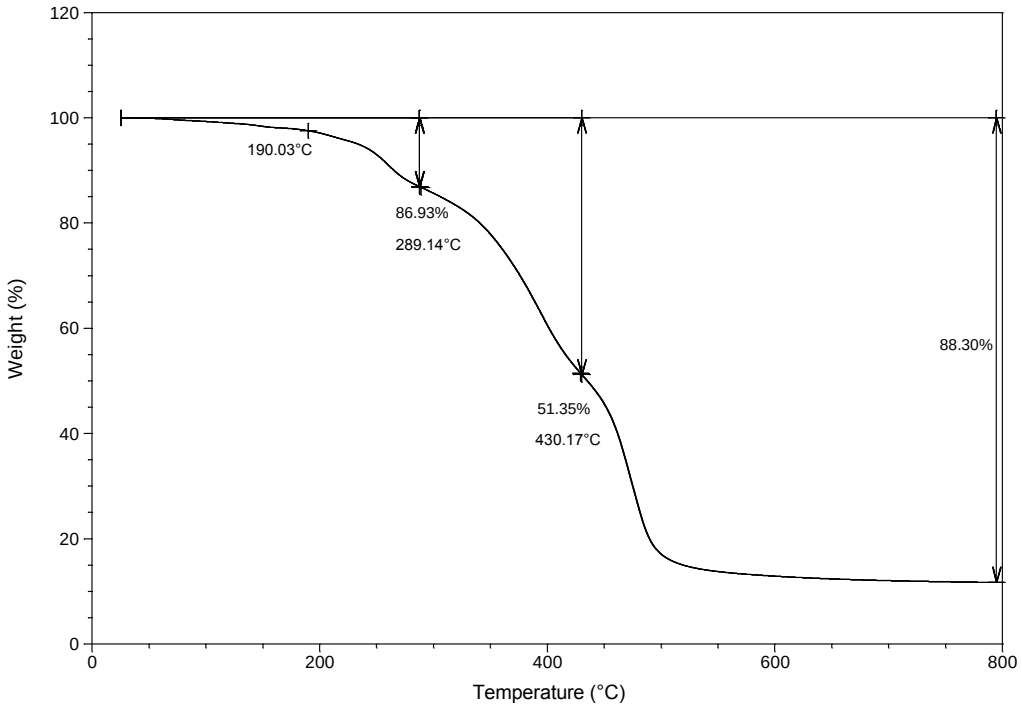

FIGURE S5 TGA trace for 6-oxoverdazyl polymer **13** from 25 to 800 °C.

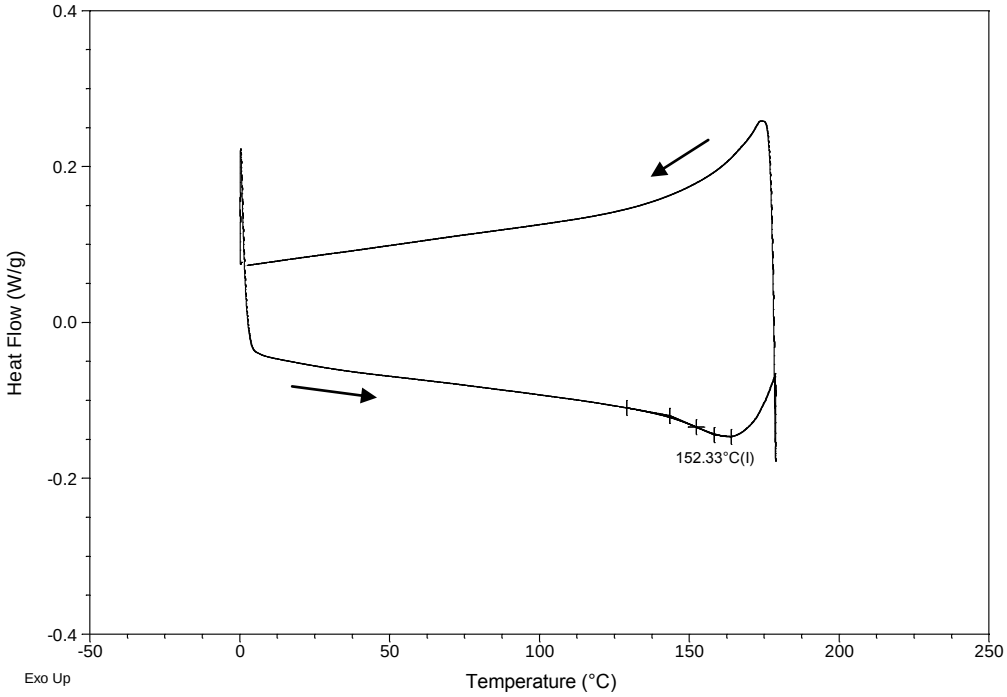

FIGURE S6 DSC data (second heating/cooling cycle) for 6-oxoverdazyl polymer **13**. The sample was heated to 180 °C followed by cooling to 0°C at a rate of 10 °C min^{-1}.

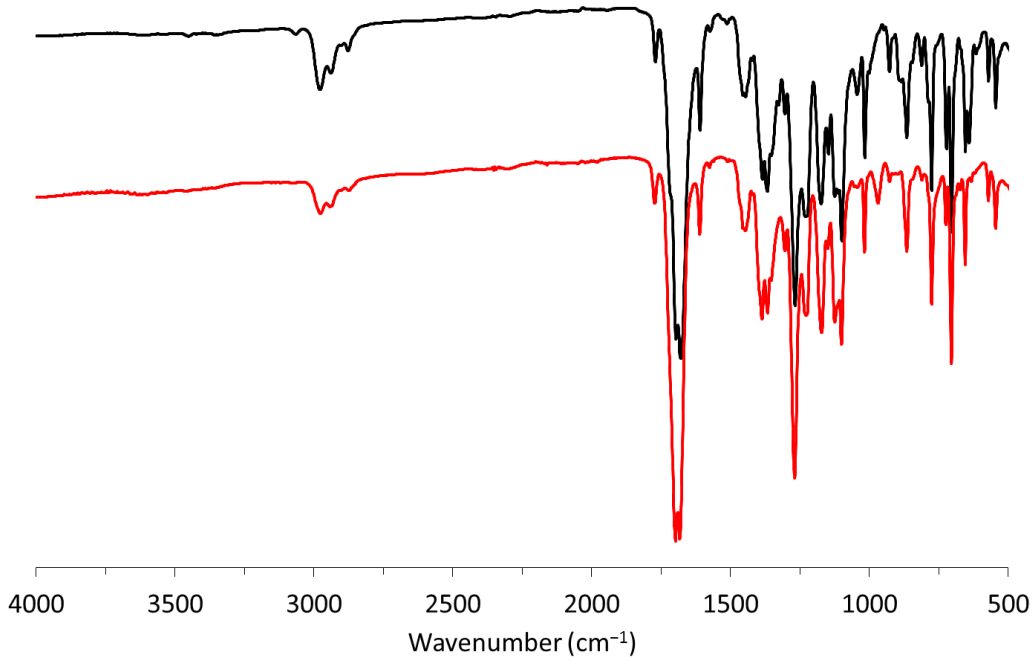

FIGURE S7 FT-IR spectra of 6-oxoverdazyl monomer **12** (red line) and polymer **13** (black line). Baselines have been offset for ease of comparison.

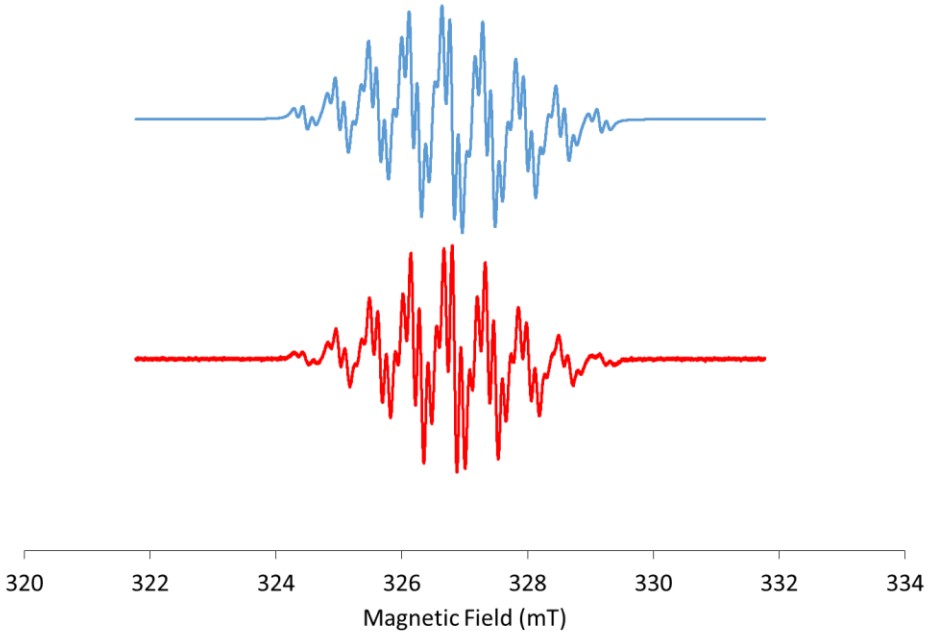

FIGURE S8 Simulated (top, blue line) and experimental (bottom, red line) EPR spectra of 6-oxoverdazyl monomer **12** in CH_2Cl_2. Parameters for simulation: g = 2.0045, line width = 0.089 mT, $a_{N1,3}$ = 0.529 mT, $a_{N2,4}$ = 0.640 mT, a_H = 0.140 mT.